



**HAL**  
open science

## Evidence for and Evaluation of Fluorine-Tellurium Chalcogen Bonding

Robin Weiss, Emmanuel Aubert, Loic Gros Lambert, Patrick Pale, Victor Mamane

► **To cite this version:**

Robin Weiss, Emmanuel Aubert, Loic Gros Lambert, Patrick Pale, Victor Mamane. Evidence for and Evaluation of Fluorine-Tellurium Chalcogen Bonding. *Chemical Science*, 2023, <10.1039/D3SC00849E>. <hal-04118408>

**HAL Id: hal-04118408**

**<https://hal.science/hal-04118408v1>**

Submitted on 6 Jun 2023

**HAL** is a multi-disciplinary open access archive for the deposit and dissemination of scientific research documents, whether they are published or not. The documents may come from teaching and research institutions in France or abroad, or from public or private research centers.

L'archive ouverte pluridisciplinaire **HAL**, est destinée au dépôt et à la diffusion de documents scientifiques de niveau recherche, publiés ou non, émanant des établissements d'enseignement et de recherche français ou étrangers, des laboratoires publics ou privés.



HAL Authorization

# Chemical Science

Accepted Manuscript

This article can be cited before page numbers have been issued, to do this please use: R. Weiss, E. Aubert, L. Gros Lambert, P. Pale and V. Mamane, *Chem. Sci.*, 2023, DOI: 10.1039/D3SC00849E.



This is an Accepted Manuscript, which has been through the Royal Society of Chemistry peer review process and has been accepted for publication.

Accepted Manuscripts are published online shortly after acceptance, before technical editing, formatting and proof reading. Using this free service, authors can make their results available to the community, in citable form, before we publish the edited article. We will replace this Accepted Manuscript with the edited and formatted Advance Article as soon as it is available.

You can find more information about Accepted Manuscripts in the [Information for Authors](#).

Please note that technical editing may introduce minor changes to the text and/or graphics, which may alter content. The journal's standard [Terms & Conditions](#) and the [Ethical guidelines](#) still apply. In no event shall the Royal Society of Chemistry be held responsible for any errors or omissions in this Accepted Manuscript or any consequences arising from the use of any information it contains.

## ARTICLE

## Evidence for and Evaluation of Fluorine-Tellurium Chalcogen Bonding

Robin Weiss,<sup>a</sup> Emmanuel Aubert,<sup>b</sup> Loïc Gros Lambert,<sup>a</sup> Patrick Pale<sup>\*a</sup> and Victor Mamane<sup>\*a</sup>Received 00th January 20xx,  
Accepted 00th January 20xx

DOI: 10.1039/x0xx00000x

In the field of noncovalent interactions, chalcogen bonding (ChB) involving the tellurium atom is currently attracting much attention in supramolecular chemistry and in catalysis. However, as a prerequisite for its application, the ChB should be studied in solution to assess its formation and, if possible, to evaluate its strength. In this context, new tellurium derivatives bearing  $\text{CH}_2\text{F}$  and  $\text{CF}_3$  groups were designed to exhibit  $\text{Te}\cdots\text{F}$  ChB and were synthesized in good to high yields. In both types of compounds,  $\text{Te}\cdots\text{F}$  interactions were characterized in solution by combining  $^{19}\text{F}$ ,  $^{125}\text{Te}$  and HOESY NMR techniques. These  $\text{Te}\cdots\text{F}$  ChBs were shown to contribute to the overall  $J_{\text{Te-F}}$  coupling constants (94–170 Hz) measured in the  $\text{CH}_2\text{F}$ - and  $\text{CF}_3$ -based tellurium derivatives. Finally, a variable temperature NMR study allowed us to approximate the energy of the  $\text{Te}\cdots\text{F}$  ChB, from 3 kJ/mol for the compounds for weak Te  $\sigma$ -holes to 11 kJ/mol for Te  $\sigma$ -holes activated by the presence of strong electron withdrawing substituents.

## Introduction

Noncovalent interactions involving halogen and more recently chalcogen atoms are increasingly of interest, especially in materials, crystal engineering, biology, in controlling molecular assembly and more recently in catalysis.<sup>1–4</sup> Highly directional attractive interactions indeed occur between an electron-rich atom (Lewis base) and an electropositive region ( $\sigma$ -hole; Fig. 1)<sup>5</sup> located at the outermost end of a  $\sigma$ -bond involving a halogen or chalcogen atom. In analogy with hydrogen bonds, these interactions were named halogen or chalcogen bond (XB or ChB, respectively).<sup>2,6</sup>

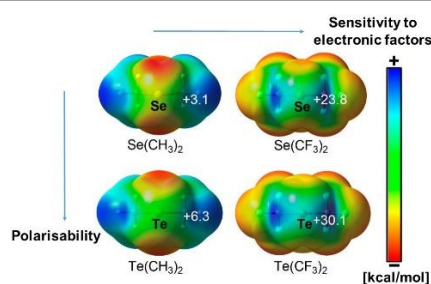


Fig. 1 Electrostatic potential maps of selected chalcogen derivatives revealing the electropositive areas, called  $\sigma$ -holes. Adapted from ref [5].

<sup>a</sup> LASYRO, UMR 7177, University of Strasbourg, 1 Rue Blaise Pascal, 67000 Strasbourg, France. E-mail: ppale@unistra.fr; vmamane@unistra.fr.

<sup>b</sup> Université de Lorraine, CNRS, CRM2, F-54000 Nancy, France

Electronic Supplementary Information (ESI) available: [Experimental procedures, characterisation data and NMR spectra; VT NMR spectra and coupling constants; computed conformational analysis and  $V_{s,\text{max}}$  data; computed NMR data; methodology for the determination of thermodynamic parameters]. See DOI: 10.1039/x0xx00000x

It is now recognized that XB, especially those involving an iodine atom, also plays a key role in biology.<sup>3a,7</sup> Furthermore, ChBs involving sulfur or selenium are now more frequently identified in biostructural and biochemical aspects.<sup>8</sup> A few tellurium compounds have also found biological applications,<sup>9</sup> but so far with no evidence of ChB involvement. On the other hand, fluorine, the most electronegative element, significantly affects the acidity or basicity, bioavailability, lipophilicity, metabolic stability and toxicity of compounds bearing it.<sup>10</sup> Thus, fluorinated compounds increasingly impact pharma- and agro-industries. For example, 28% of newly approved drugs in the last decade (2011–2020) are fluorinated.<sup>10</sup> With its high electronegativity, fluorine is an HB acceptor,<sup>11</sup> but not an XB donor unlike other halogens.<sup>12</sup> Thus, combining both tellurium and fluorine seems worth investigating.<sup>13</sup> However, noncovalent interactions involving fluorine as acceptor in a ChB remains almost unknown,<sup>14</sup> especially the  $\text{Te}\cdots\text{F}$  interaction.

The extent of a  $\sigma$ -hole on an atom increases with its polarizability and decreases with its electronegativity (Fig. 1).<sup>15</sup> Therefore, iodine is the most effective XB donor,<sup>16</sup> and tellurium species should have the strongest ChB property.<sup>17</sup> In this respect, several studies on tellurium compounds in solution<sup>18</sup> focused on  $\text{Te}\cdots\text{O}$ ,<sup>19</sup>  $\text{Te}\cdots\text{N}$ ,<sup>20</sup>  $\text{Te}\cdots\text{Ch}$ ,<sup>21</sup> and  $\text{Te}\cdots\text{Pnictogen}$ <sup>22</sup> interactions (Fig. 2, top). Despite their detection in some cases in the solid state,<sup>4a,23</sup>  $\text{Te}\cdots\text{F}$  interactions have been scarcely studied in solution.<sup>24</sup> In particular, Zhao and Gabbai reported the recognition of a fluoride anion by 2-boronylnaphtyl telluronium, however the presence of a covalent bond was finally established with such bidentate compounds.<sup>24a</sup>

This context urges us to identify  $\text{Te}\cdots\text{F}$  interaction and to characterize the corresponding property.



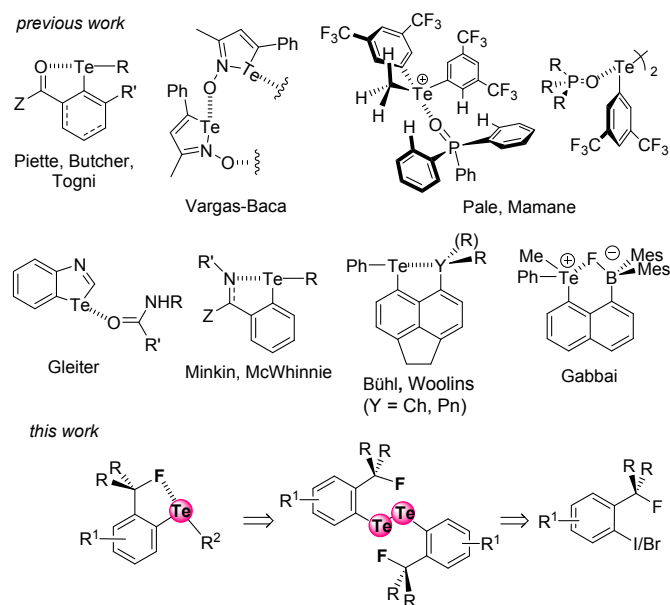


**Fig. 2** The known noncovalent interactions involving tellurium atoms, and the first  $\text{Te}\cdots\text{F}$  interaction described here.

In continuation of our recent XB and ChB studies and applications in medicinal chemistry,<sup>25</sup> enantioseparation,<sup>26</sup> and organocatalysis,<sup>19b,27</sup> we have now designed two series of fluorinated *ortho*-tolyl telluride derivatives to identify  $\text{Te}\cdots\text{F}$  interactions and to characterize their corresponding properties. We report here the first evidence of a  $\text{Te}\cdots\text{F}$  interaction (ChB) in solution, as well as an evaluation of its strength (Fig. 2, bottom).

## Results and discussion

### Probe design

The choice of fluorinated *ortho*-tolyl telluride derivatives as a  $\text{Te}\cdots\text{F}$  probe was motivated by three factors. First, a  $\text{Te}\cdots\text{F}$  interaction should influence the rotational barrier of the fluoromethyl substituent and related groups. Second, the probe provides an opportunity to monitor the presence of rotational isomers by combining  $^{19}\text{F}$  and  $^{125}\text{Te}$  NMR, and thus to evaluate the strength of the  $\text{Te}\cdots\text{F}$  interaction. Finally,  $\text{Te}$   $\sigma$ -hole(s) can be tuned by appropriate electron-withdrawing or -donating substituent(s) either on the tolyl moiety or on the other  $\text{Te}$  substituent ( $\text{R}^1$ ,  $\text{R}^2$  respectively in Fig. 2, bottom left). The simplest *ortho*-fluoromethylphenyl telluride ( $\text{CH}_2\text{F}$  series) must exhibit at least two rotamers: one (*syn*- $\text{CH}_2\text{F}$ ) where tellurium and fluoride atoms are close to one another and a second (*anti*- $\text{CH}_2\text{F}$ ) in which the fluoride could be far from the tellurium atom (Fig. 3A). Obviously, an intramolecular  $\text{Te}\cdots\text{F}$  interaction would only exist in *syn*- $\text{CH}_2\text{F}$  and, if so and strong enough, this interaction could shift the conformational equilibrium towards this *syn*-conformer. Furthermore, the latter should exhibit different chemical shifts in  $^{19}\text{F}$  and  $^{125}\text{Te}$  NMR due to electron density transfer from F to Te depending on the  $\text{Te}\cdots\text{F}$  interaction strength. Coupling constants could also be helpful because both  $^{19}\text{F}$  and  $^{125}\text{Te}$  exhibit  $\frac{1}{2}$  nuclear spin. In addition to

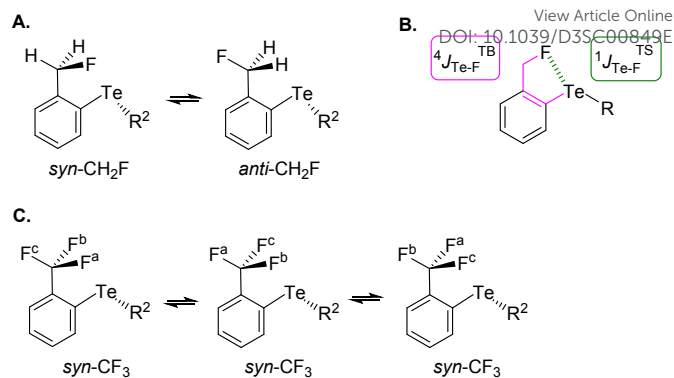


**Fig. 3** (A) The more stable *syn* and *anti* conformations for the  $\text{CH}_2\text{F}$  series. (B) Through bond (TB) and through space (TS) coupling for the *syn* conformation in the  $\text{CH}_2\text{F}$  series. (C) Permanent *syn* conformation in the  $\text{CF}_3$  series.

the through-bond coupling constant ( $^4J_{\text{Te-F}}^{\text{TB}}$ ), a through-space contribution ( $^1J_{\text{Te-F}}^{\text{TS}}$ ) to the overall coupling constant ( $^4J_{\text{Te-F}}$ ) should arise in *syn*- $\text{CH}_2\text{F}$  if  $\text{Te}\cdots\text{F}$  interaction is present (Fig. 3B).<sup>28</sup> Therefore,  $^{19}\text{F}$  and  $^{125}\text{Te}$  NMR monitoring could reveal such differences and provide information on the conformational equilibrium and its evolution.

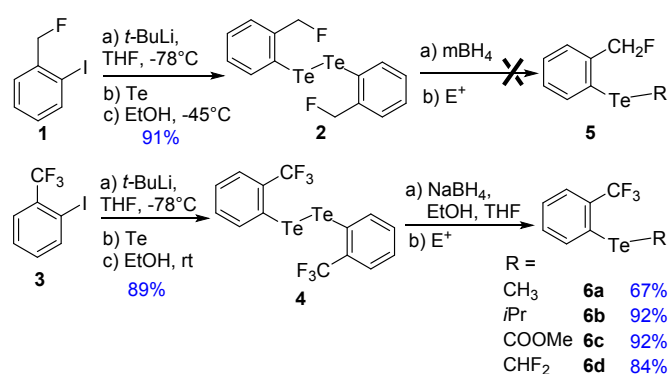
In contrast, the *ortho*-trifluoromethylphenyl telluride ( $\text{CF}_3$  series) will always have one fluoride facing or close to the tellurium atom (Fig. 3C). Therefore, depending on the strength of the  $\text{Te}\cdots\text{F}$  interaction, two possibilities could arise: this interaction could either lock the rotation of the  $\text{CF}_3$  group and thus render the fluoride atoms non-equivalent in NMR, or could be averaged over the  $\text{CF}_3$  group.

### Synthesis

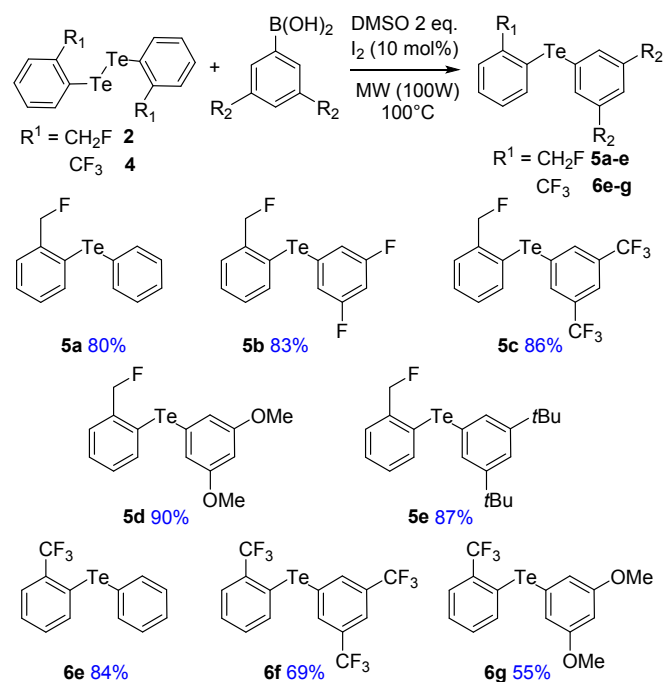
To address these issues, we prepared two series of *ortho*-tolyl tellurides bearing either a fluoromethyl or a trifluoromethyl group (Schemes 1 and 2). Starting from fluoromethyl-2-iodobenzene **1**, iodine-lithium exchange followed by trapping with grey tellurium gave the corresponding lithium telluride,<sup>29</sup> which upon quenching under air provided in high yield the corresponding diaryl ditelluride **2**<sup>30</sup> (Scheme 1, top). Applying the same strategy to iodo-2-trifluoromethylbenzene **3** gave the trifluoromethyl analogue **4** in similar yield.<sup>19a</sup> Upon reductive cleavage and trapping of the resulting tellurate by electrophiles, ditelluride **2** afforded mixtures in which the expected tellurides **5** could not be detected, independent of the nature of the borohydride or electrophile (Scheme 1, top). In contrast, treatment of ditelluride **4** with  $\text{NaBH}_4$  and subsequent electrophilic quenching readily gave the expected alkyl aryl tellurides **6a-c** with good to high yields. Under these conditions, using  $\text{CF}_2\text{Br}_2$  as the electrophile resulted only in the debrominated product **6d** (Scheme 1, bottom).

A more general route to both tellurides **5** and **6** was achieved by a microwave-promoted coupling reaction with various arylboronic acids (Scheme 2).<sup>31</sup> To tune the expected ChB intensity, a series of boronic acid derivatives carrying electron-rich or electron-poor substituents was employed in this coupling to provide the corresponding diaryl tellurides **5a-e** and **6e-g** in good to high yields. These compounds could be stored at  $4^\circ\text{C}$  for several months without degradation. Moreover, the





Scheme 1 Synthesis of a series of fluorinated alkyl aryl tellurides



Scheme 2 Synthesis of a series of fluorinated diaryl tellurides

diarylditellurides showed good stability in solution at room temperature for several days with no particular precautions. In contrast, alkyl aryl tellurides **6a-d** were very sensitive to oxygen and light, causing rapid decomposition in solution with formation of a grey metallic deposit, probably corresponding to tellurium(0).<sup>32</sup> Unfortunately, all of the prepared tellurides **5** and **6** were viscous oils that could not be crystallized.

### Electrostatic surface potential (ESP) analysis

For ESP analysis, compounds **5a**, **5c** and **6e**, **6f** were chosen as representative members of respectively the CH<sub>2</sub>F and CF<sub>3</sub> series. Their molecular geometries were optimized by DFT (B3LYP/Def2TZVPP, see ESI §IV.B for details). As anticipated for the CH<sub>2</sub>F series, the *syn*-CH<sub>2</sub>F and *anti*-CH<sub>2</sub>F conformations were found to be the most stable ones among all possible conformations for both **5a** and **5c** (see ESI, Fig. S10 and Table 8). Coherently, only one stable conformation was detected for **6e** and **6f** (Fig. 3C and ESI, Fig. S10 and Table 9). The  $V_{s,max}$  extrema were then characterized for each conformation of **5a** and **5c**

(see ESI, Tables S8-S9 and Figure S11). Interestingly, only one  $\sigma$ -hole was detected in the *syn* conformers in the elongation of the bond between Te and the aromatic group bearing CH<sub>2</sub>F. The other  $\sigma$ -hole that was expected to be facing the fluorine atom could not be characterized. The latter  $\sigma$  hole could be detected in the *anti* conformer, however. These results suggest a possible through-space electron delocalization from fluorine to a tellurium  $\sigma$ -hole in the *syn* conformer. This hypothesis was further supported by the topological analysis of the DFT calculated electron density, where a bond path is observed between F and Te atoms with a small but non-negligible delocalization index of about 0.065 (see ESI, Figure S12 and Table S10). Similar data were obtained with compounds **6e** and **6f** (see ESI, Table S10).

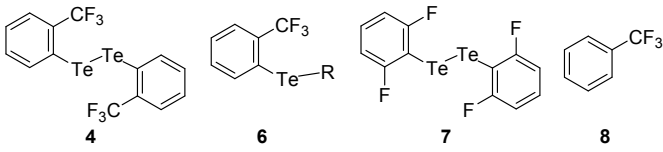
### Te•••F interaction in solution

The mono- and trifluorotolyl tellurides **5a-e** and **6a-g**, as well as their ditelluride precursors **2** and **4**, were then studied in solution, using <sup>19</sup>F and <sup>125</sup>Te NMR to probe the presence or absence of  $\sigma$ -hole Te•••F interactions (see spectra in ESI, §V). The trifluorotolyl tellurium derivatives **6a-g** exhibit similar chemical shifts in <sup>19</sup>F NMR (-61 ± 1 ppm), but a large shift range in <sup>125</sup>Te NMR (369-795 ppm) (Table 1). The latter are nevertheless typical of divalent tellurides,<sup>33</sup> as observed in the <sup>19</sup>F and <sup>125</sup>Te NMR spectra of **4** (-60.5 ppm and 438.1 ppm, respectively). The <sup>125</sup>Te signal appears as a quadruplet, indicating a <sup>4</sup>J<sub>Te-F</sub> coupling with the three fluorine atoms of the trifluoromethyl group. This quadruplet also reveals the magnetic equivalence of these fluorine atoms, and thus the free rotation of the trifluoromethyl group at room temperature and even at -80 °C. Interestingly, these <sup>4</sup>J<sub>Te-F</sub> coupling constants (94-154 Hz, Table 1) are far lower than those observed for covalent Te-F bonds (950 Hz).<sup>24,34</sup> Nevertheless, they are two to four times higher than <sup>3</sup>J<sub>Te-F</sub> coupling values in the 2,6-difluorophenylditelluride **7** (45 Hz), used for comparison purposes. Such a counter-intuitive difference was observed in various fluorinated compounds<sup>35</sup> and in hydrogen bonds involving fluorine.<sup>36</sup> The underlying phenomenon was ascribed to through-space orbital overlap,<sup>37</sup> and non-linearly correlated to the distance of the interacting atoms, and thus to the strength of the interaction.<sup>35b</sup> The latter could be assessed from the good linear correlation between <sup>19</sup>F chemical shifts ( $\delta_F$ ) and <sup>4</sup>J<sub>Te-F</sub> coupling constants (Fig. 4). This correlation revealed that more shielded  $\delta_F$  correspond to higher <sup>4</sup>J<sub>Te-F</sub> values, and therefore to stronger interactions.

Furthermore, <sup>19</sup>F NMR chemical shifts of **4** and **6a-g** (-61 ± 1 ppm) were higher than that of trifluorotoluene **8** (-63.8 ppm), independent of the Te substituent. This deshielding is mostly due to the presence of tellurium and indicates a modification of fluorine polarization, as expected from an interaction between the F lone pair and Te  $\sigma$ -holes. These combined observations strongly suggest the presence of noncovalent Te•••F interactions in this series of Te compounds.

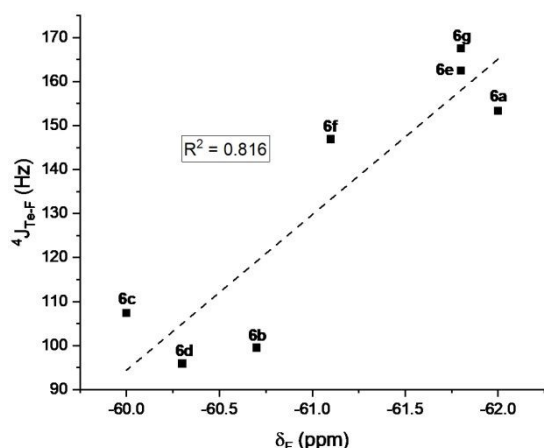
Unexpected observations in <sup>13</sup>C NMR corroborate this possibility. The alkyl aryl tellurides **6a-d** exhibit what appears as a <sup>5</sup>J<sub>C-F</sub> coupling between the Te-bound alkyl, aryl or carboxylate



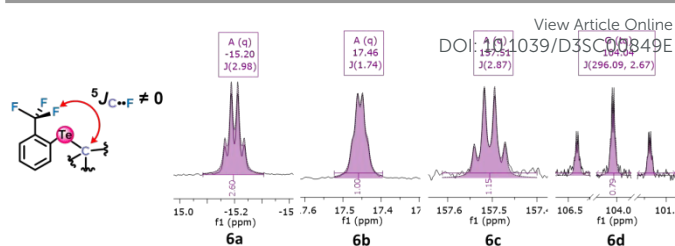
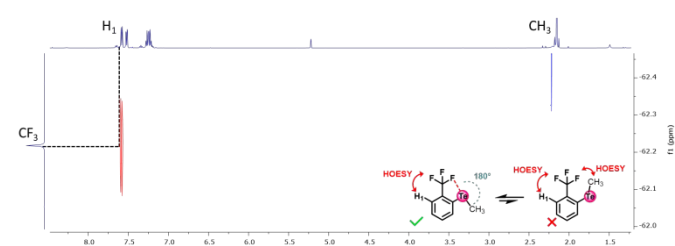
**Table 1**  $^{125}\text{Te}$  and  $^{19}\text{F}$  NMR chemical shifts and Te-F coupling constants from tellurium derivatives **4** and **6a-g** compared to the ditelluride **7** and trifluorotoluene **8**.<sup>a</sup>


Tellurium (R)	$\delta_{\text{Te}}$ (ppm)	$\delta_{\text{F}}$ (ppm)	$^3J_{\text{Te-F}}$ (Hz)	$^4J_{\text{Te-F}}$ (Hz)	$^5J_{\text{C-F}}$ (Hz)
<b>4</b>	438.1	-60.5	-	170.2	-
<b>6a</b> (CH <sub>3</sub> )	369.4	-62.0	-	153.3	2.98
<b>6b</b> ( <i>i</i> Pr)	720.7	-60.7	-	99.5	1.74
<b>6c</b> (COOMe)	795.5	-60.0	-	107.4	2.87
<b>6d</b> (CF <sub>2</sub> H)	- <sup>b</sup>	-60.3	-	95.9 <sup>c</sup>	2.67
<b>6e</b> (Ph)	728.2	-61.8	-	162.5	-
<b>6f</b> (3,5-(CF <sub>3</sub> ) <sub>2</sub> Ph)	779.5	-61.1	-	146.9	-
<b>6g</b> (3,5-(MeO) <sub>2</sub> Ph)	760.1	-61.8	-	167.5	-
<b>7</b>	215.6	-86.2	45.5	-	-
<b>8</b>	-	-63.8	-	-	-

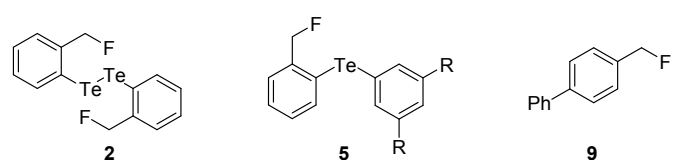
<sup>a</sup> Conditions: tellurium species (5-20 mM) in CDCl<sub>3</sub> at 25 °C. <sup>b</sup> The product decomposed during the acquisition of the  $^{125}\text{Te}$  NMR spectrum. <sup>c</sup> Measured on the  $^{19}\text{F}$  spectrum.

**Fig. 4** Correlation between  $^{19}\text{F}$  NMR chemical shifts of the tellurides **6a-g** and  $^4J_{\text{Te-F}}$  coupling constants.

carbon bonded to the tellurium atom and the fluorine atoms (Fig. 5). Despite the large number of bonds separating them and the presence of the tellurium atom, the observed coupling constants were unexpectedly high (1.74-2.98 Hz; see Table 1). These values are usually typical of  $^3J_{\text{C-F}}$  couplings.<sup>38</sup> Such coupling<sup>39</sup> could be due to noncovalent Te•••F interactions, and if so, the Te  $\sigma$ -hole involved in should impose a configuration in which the Te substituent would be aligned with the Te•••F interaction in an *anti* position (see drawing in Fig. 6). To verify this hypothesis, a  $^1\text{H}$ - $^{19}\text{F}$  HOESY NMR experiment was performed with the methyl-substituted telluride **6a** (Fig. 6). This experiment revealed that the methyl is not close to the CF<sub>3</sub> group, whereas the latter is close to the *ortho*-proton of the phenyl moiety. Therefore, the methyl group should be oriented away from the CF<sub>3</sub> group in solution. Such observations further corroborate the presence of a Te•••F interaction.

**Fig. 5** Fragments of tellurides **6a-d**  $^{13}\text{C}$  NMR spectra revealing the  $^5J_{\text{C-F}}$  due to coupling between the carbon bonded to the tellurium atom and the fluorine atoms.**Fig. 6** HOESY spectrum of telluride **6a** in CD<sub>2</sub>Cl<sub>2</sub>

The monofluorotolyl tellurides **5a-e** were then investigated under the same NMR conditions (Table 2).  $^{125}\text{Te}$  NMR chemical shifts (345-645 ppm) were again in the classical range for divalent tellurides.<sup>33</sup> As for the CF<sub>3</sub> series,  $^{19}\text{F}$  NMR chemical shifts of **2** and **5a-e** (-204  $\pm$  1 ppm) were higher than that of the reference compound **9** (-206.1 ppm). A long-range  $^4J_{\text{Te-F}}$  coupling between the fluorine and tellurium atoms was also observed as a doublet in this series, with similar values (104.6-129.6 Hz). The latter are nevertheless lower than in the CF<sub>3</sub> series, as are the  $^{125}\text{Te}$  chemical shifts (see **5a** vs **6e**, **5c** vs **6f**, **5d** vs **6g** and **2** vs **4**). Both facts further support the presence of a Te•••F  $\sigma$ -hole-based interaction for the same reason. Because the deepness of a  $\sigma$ -hole is directly affected by adjacent electron-withdrawing or -donating substituent(s) (see Fig. 1), we attempted to tune Te  $\sigma$ -holes by selecting typical substituents at the *meta* position of the Te aryl moiety (**5b-e** vs **5a**) in this more structurally homogeneous series.

**Table 2**  $^{125}\text{Te}$  and  $^{19}\text{F}$  NMR chemical shifts and Te-F coupling constants from tellurium derivatives **2** and **5a-e** compared to the monofluorotoluene **9**.<sup>a</sup>


Tellurium (R)	$\delta_{\text{Te}}$ (ppm)	$\delta_{\text{F}}$ (ppm)	$^4J_{\text{Te-F}}$ (Hz)
<b>2</b>	345.6	-203.2	129.6
<b>5a</b> (H)	596.4	-205.3	110.4
<b>5b</b> (F)	644.8	-204.3	108.7
<b>5c</b> (CF <sub>3</sub> )	645.1	-202.3	127.0
<b>5d</b> (OMe)	622.8	-205.3	108.8
<b>5e</b> ( <i>t</i> Bu)	594.3	-205.5	108.5
<b>9</b>	-	-206.1	-

<sup>a</sup> Conditions: tellurium species (20 mM) in CDCl<sub>3</sub> at 25 °C.



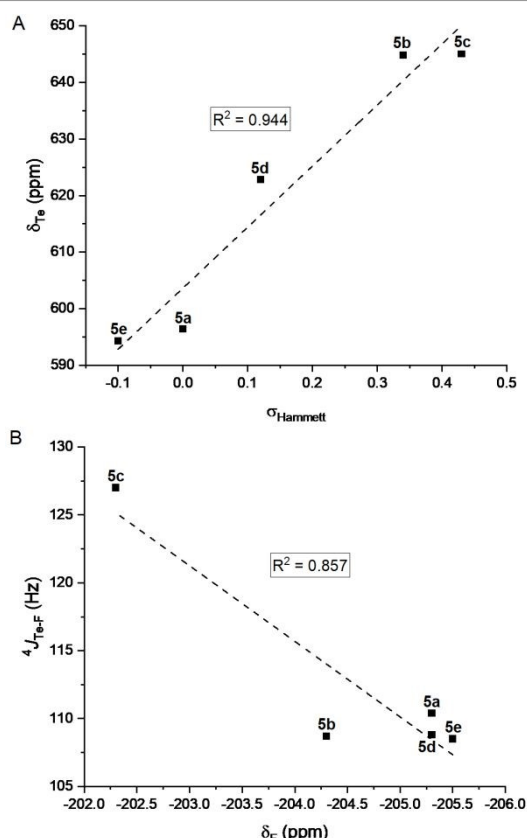


**Fig. 7** (A) Correlation between  $^{125}\text{Te}$  NMR chemical shifts of the tellurides **5a-e** and Hammett parameters. (B) Correlation between  $^4J_{\text{Te-F}}$  coupling constants and  $^{19}\text{F}$  NMR chemical shifts.

Rewardingly, the electronic effect ( $\sigma_m$ ) of these meta substituents could clearly be correlated to  $^{125}\text{Te}$  chemical shifts (Fig. 7A). Moreover,  $^{19}\text{F}$  chemical shifts correlated with the  $^4J_{\text{Te-F}}$  coupling constants (Fig. 7B) and showed that the more electron-withdrawing substituent induced the largest  $^4J_{\text{Te-F}}$  coupling, as expected for a  $\sigma$ -hole-based interaction. These effects confirmed that the  $^4J_{\text{Te-F}}$  value represents a measure of the strength of the noncovalent  $\text{Te}\cdots\text{F}$  interaction.

#### Contribution of the $\text{Te}\cdots\text{F}$ ChB to the overall $^4J_{\text{Te-F}}$

Two different studies were performed in order to confirm the role of the  $\text{Te}$   $\sigma$ -hole in the  $\text{Te}\cdots\text{F}$  interaction and to estimate the ChB contribution to the overall coupling constant.

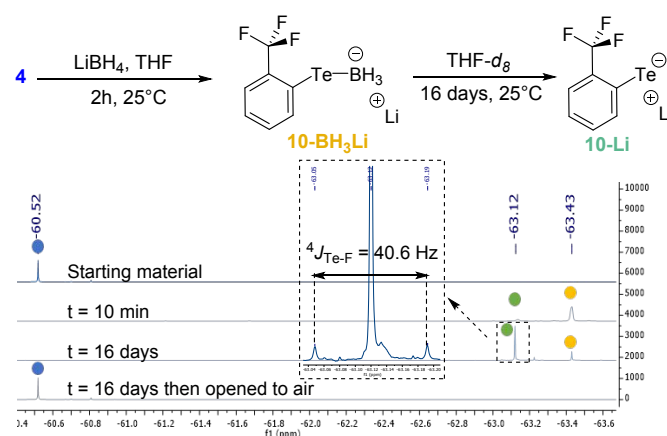
In the first study, the lithium tellurolate intermediate **10-TeLi**, where the negative charge on  $\text{Te}$  was expected to reduce the involvement of its  $\sigma$ -hole in the  $\text{Te}\cdots\text{F}$  interaction, was prepared (Scheme 3). The characterization of **10-TeLi** by NMR and in particular the determination of the  $\text{Te-F}$  coupling constant should provide an approximate assessment of the through-space coupling due to chalcogen bonding.

Lithium tellurolate **10-TeLi** was obtained by slow decomposition of **10-TeBH<sub>3</sub>Li**. The latter was generated by reaction of ditelluride **4** with an excess of  $\text{LiBH}_4$  in THF.<sup>40</sup> The decomposition of **10-TeBH<sub>3</sub>Li** to **10-TeLi** was monitored by  $^{19}\text{F}$  NMR in THF-*d*<sub>8</sub> (Scheme 3 and ESI for full characterizations). Almost full conversion was observed after 16 days with complete disappearance of the boron signal of **10-TeBH<sub>3</sub>Li** in  $^{11}\text{B}$  NMR and

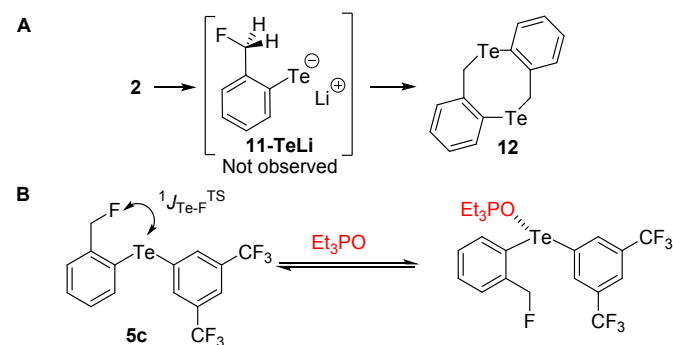
the appearance of a new  $^{125}\text{Te}$  signal for **10-TeLi** (see ESI)<sup>41</sup> Moreover, ditelluride **4** was recovered by oxidation of **10-TeLi** after opening the NMR tube to air. These observations proved that **10-TeLi** was formed after 16 days. The  $\text{Te-F}$  coupling constant of 40.6 Hz measured for **10-TeLi** was much lower than the  $^4J_{\text{Te-F}}$  values observed for tellurides **6a-g** (Table 1). Such large difference between the telluride and the tellurolate should at least partly reveal the through-space contribution and thus indicates a contribution of the  $\text{Te}\cdots\text{F}$  ChB to the overall  $^4J_{\text{Te-F}}$  in compounds **6a-g**.

Similarly, we attempted to form the analogous tellurolate **11-TeLi** but all attempts failed, probably because it dimerized to tellurocine **12** (Scheme 4A).<sup>30</sup>

In the second study, the  $^4J_{\text{Te-F}}$  evolution of tellurides in the presence of  $\text{Et}_3\text{PO}$  Lewis base was investigated by NMR. The tellurides were expected to form intermolecular  $\text{Te}\cdots\text{O}$  interaction in competition with the intramolecular  $\text{Te}\cdots\text{F}$  ChB with a direct influence on  $^4J_{\text{Te-F}}$  (Scheme 4B). This strategy was tested on telluride **5c** with the strongest  $\text{Te}\cdots\text{F}$  ChB, and to avoid a possible hydrogen bond between  $\text{Et}_3\text{PO}$  and  $\text{CDCl}_3$ , the competition experiments were performed in deuterated cyclohexane.<sup>19a</sup> Large variations of  $^4J_{\text{Te-F}}$  were obtained after addition of 1, 5 and 10 equiv. of  $\text{Et}_3\text{PO}$  ( $\Delta^4J_{\text{Te-F}} = -7.8$ ,  $-24.3$  and  $-32.8$  Hz, respectively) and a plateau ( $\sim 33$  Hz) was reached between 10 and 20 equiv. of Lewis base (see ESI for details).



**Scheme 3** Preparation of lithium tellurolates **10-TeLi** and  $^{19}\text{F}$  NMR monitoring (color code: **4** in blue, **10-TeBH<sub>3</sub>Li** in yellow and **10-TeLi** in green)



**Scheme 4** A) Attempted preparation of tellurolate **11-TeLi**. B) Competition experiments between **5c** and  $\text{Et}_3\text{PO}$ .



At this plateau, the intramolecular Te•••F interaction was completely replaced by the intermolecular Te•••O interaction. Therefore, the difference of about 33 Hz should reflect the contribution of the Te•••F ChB to the overall  $^4J_{\text{Te-F}}$  value.

This strategy was unsuccessful when applied to telluride **6f**. Indeed, no modification of  $^4J_{\text{Te-F}}$  was observed after addition of 1 equiv. of Et<sub>3</sub>PO and only small variations were observed when 5 or 10 equiv. were employed ( $\Delta^4J_{\text{Te-F}} = -3.7$  and  $-5.9$  Hz, respectively) (see ESI for details). These variations represent only 2.4 and 3.9% of the  $^4J_{\text{Te-F}}$  value before addition of the Lewis base, suggesting that the Te•••F interaction is strong enough in telluride **6f** to outweigh the competition from an intermolecular Lewis base such as Et<sub>3</sub>PO.

### Evaluating the strength of Te•••F interaction in solution for compounds **5**

As determined above, the measured  $^4J_{\text{Te-F}}$  coupling may reflect the noncovalent Te•••F interaction strength, but its value is averaged over the various conformations. Based on our conformational analysis, the *syn* and *anti* conformers are the major ones; we can reasonably assume a two state equilibrium model in which the  $^4J_{\text{Te-F}}$  coupling results from the relative proportion of each conformation contribution  $^4J_{\text{Te-F}(\textit{syn})}$  and  $^4J_{\text{Te-F}(\textit{anti})}$  (equation 1;  $\chi_{\textit{syn}}$  is a temperature-dependent variable representing the relative population of *syn* conformer).

$$^4J_{\text{Te-F}} = \chi_{\textit{syn}}(^4J_{\text{Te-F}(\textit{syn})}) + (1 - \chi_{\textit{syn}})(^4J_{\text{Te-F}(\textit{anti})}) \quad (\text{Eq. 1})$$

This expression can be inserted into equation 2, which defines the *anti-syn* equilibrium constant  $K_A$  to give equation 3.

$$K_A = \chi_{\textit{syn}} / (1 - \chi_{\textit{syn}}) \quad (\text{Eq. 2})$$

$$K_A = (^4J_{\text{Te-F}} - ^4J_{\text{Te-F}(\textit{anti})}) / (^4J_{\text{Te-F}(\textit{syn})} - ^4J_{\text{Te-F}}) \quad (\text{Eq. 3})$$

The Gibbs free energy of this equilibrium is thus expressed as a function of coupling constants and of temperature (equation 4).

$$\Delta G = \Delta H - T\Delta S = -RT \ln K_A \\ = -RT \ln [(^4J_{\text{Te-F}} - ^4J_{\text{Te-F}(\textit{anti})}) / (^4J_{\text{Te-F}(\textit{syn})} - ^4J_{\text{Te-F}})] \quad (\text{Eq. 4})$$

To evaluate the  $^4J_{\text{Te-F}}$  values as a function of the conformation, relativistic DFT calculations were performed on each conformer. These calculations provided large negative values for  $^4J_{\text{Te-F}}$  ( $-249 \pm 4$  Hz for **5a-5c**;  $-164 \pm 2$  Hz for **6e-6f**) and a much smaller positive value for  $^4J_{\text{Te-F}(\textit{anti})}$  ( $+19$ - $20$  Hz) (see ESI §IV.D, Table S11). Surprisingly, a related study with fluoroseleno compounds suggested that  $^4J_{\text{Te-F}(\textit{anti})}$  was approximately zero because no Se•••F coupling was detected in selenolate **11-TeLi**, which was considered to be in an *anti* conformation due to electronic repulsion (Scheme 4).<sup>14</sup> This could not be confirmed on the analogous tellurostate **11-TeLi** because of its instability (Scheme 4A).<sup>30</sup> We nevertheless performed relativistic DFT calculations for **11-TeLi**, along all the C-C-C-F torsion angles from the *anti* to the *syn* conformer. The resulting data showed that  $^4J_{\text{Te-F}(\textit{anti})}$  remains relatively constant ( $20 \pm 10$ Hz) from the *anti* to a  $90^\circ$  arrangement and then sharply decreases to  $-130$  Hz for the *syn* conformer (see ESI §IV.D, Figure S13). All of the computed data showed that  $^4J_{\text{Te-F}(\textit{anti})}$  is close to 20 Hz, independent of the telluronium structure (**11-TeLi** and **2**, **5a** and **5c** (see ESI §IV.D, Figure S13 and Table S11).

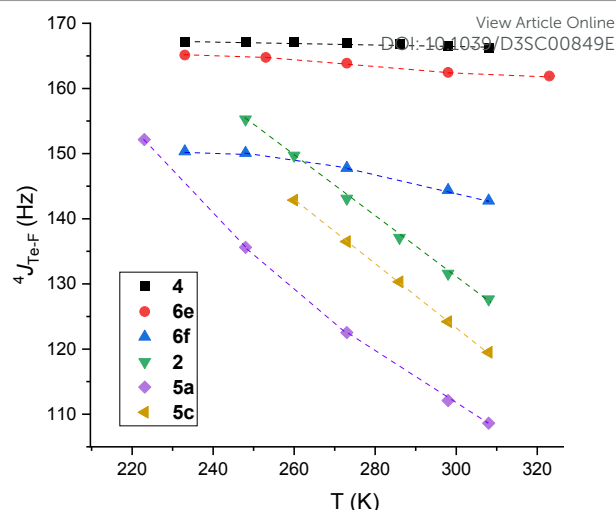


Fig. 8 Evolution of  $^4J_{\text{Te-F}}$  of trifluorotolyl (**2**, **6e** and **6f**) and monofluorotolyl (**4**, **5a** and **5c**) derivatives as a function of temperature.

To obtain experimental data on  $^4J_{\text{Te-F}}$ , and in order to assess thermodynamic parameters, typical mono- and trifluorotolyl tellurium derivatives (**2**, **4**, **5a**, **6e**, **5c** and **6f**) were examined by variable temperature (VT) NMR from 233 to 308K (Fig. 8 and ESI, §III.A and III.B). The trifluoro compounds were studied as models with permanent *syn* conformations in order to verify the non-dependency of  $^4J_{\text{Te-F}(\textit{syn})}$  with temperature.

Low variations of  $^4J_{\text{Te-F}}$  were obtained for the trifluorotolyl derivatives (variation for **4**: 0.7%; **6e**: 2.6%; **6f**: 6.9%) proving that  $^4J_{\text{Te-F}}$  is almost independent of temperature (see ESI, §III.A for complete data). In contrast, the monofluorotolyl compounds (**2**, **5a** and **5c**) showed large variations ( $\Delta^4J_{\text{Te-F}}$  up to 44 Hz), as expected from temperature-dependent modification of the *anti-syn* equilibrium. Interestingly, the highest value was observed for the 3,5-bis(trifluoromethyl)phenyl derivative **5c** that exhibits the largest Te  $\sigma$ -hole (Fig. 8 and ESI, §III.B). Similarly,  $\delta_F$  displayed a net deshielding upon decreasing the temperature for the monofluorotolyl derivatives ( $\Delta\delta_F \sim 4$  ppm, Tables S4-S6 in ESI), but a slight shielding for the trifluorotolyl analogs ( $\Delta\delta_F \sim 0.5$  ppm) (Tables S1-S3 in ESI). Such effects are in line with an increased electron density transfer from an F lone pair to the Te  $\sigma$ -hole in the monofluorotolyl series, as expected from increasing predominance of the *syn* conformer.

Based on the results at low temperature, the enthalpy of the *anti-syn* equilibrium seems to be mostly driven by the Te•••F interaction. Therefore, this enthalpy can be estimated from the energy of the Te•••F interaction using equation 5:

$$\Delta H \approx E_{\text{Te}\cdots\text{F}} \quad (\text{Eq. 5})$$

From the experimental VT NMR data,  $\Delta H$  and  $\Delta S$  of eq. 4 were determined as follows. Assuming a two state model, we first determined the values of  $^4J_{\text{Te-F}(\textit{anti})}$  and  $^4J_{\text{Te-F}(\textit{syn})}$  that give the best linearity of  $-RT \ln K_A$  as a function of T. Due to poor convergence, one of the two parameters was fixed while refining the second one. We thus chose to solve eq. 4 for two different fixed values of  $^4J_{\text{Te-F}(\textit{anti})}$ , namely  $-20$  Hz and  $+20$  Hz because these values represent the average theoretical calculations for  $^4J_{\text{Te-F}(\textit{anti})}$  (see above) and because positive and negative coupling constants were calculated for non-*syn* conformations. The optimal value



of  $^4J_{\text{Te-F(syn)}}$  was then determined, leading to a linear fit and values of  $\Delta H$  and  $\Delta S$  that were obtained as intervals corresponding to the positive and negative estimated values of  $^4J_{\text{Te-F(anti)}}$  (see ESI §III.C and Table S7). The estimated values of  $\Delta H$  and  $\Delta S$  were then used to calculate  $E_{\text{Te}\cdots\text{F}}$  and  $\Delta G^{298}$  (Table 3). For compounds **2** and **5c**, the obtained negative  $\Delta G^{298}$  values for the *anti*  $\rightleftharpoons$  *syn* equilibrium indicated a favorable shift towards the *syn* conformer, and thus confirmed the preference in solution for the conformer exhibiting a  $\sigma$ -hole  $\text{Te}\cdots\text{F}$  interaction. On the contrary, the positive value of  $\Delta G^{298}$  obtained for compound **5a** indicated that the *anti* conformer is the major component in solution at room temperature. This result revealed the strong influence of the presence of electron-withdrawing substituents, which increase the deepness of the Te  $\sigma$ -hole, and thus the  $\text{Te}\cdots\text{F}$  interaction, as recently demonstrated for related  $\sigma$ -hole interactions involving tellurium atoms.<sup>17a,b</sup>

This effect is also reflected by the more negative entropy of compound **5c** compared to **5a** ( $-26.0$  vs  $-18.9$   $\text{J}\cdot\text{K}^{-1}\cdot\text{mol}^{-1}$ ). Here again, the increased deepness of the Te  $\sigma$ -hole strengthens the  $\text{Te}\cdots\text{F}$  interaction, which in turn increases the proportion of *syn* conformer and reduces the molecular degree of freedom. The energies of these  $\text{Te}\cdots\text{F}$  interactions are modest ( $-3$  to  $-11$   $\text{kJ}\cdot\text{mol}^{-1}$ ), and slightly lower than the well-known  $\text{Te}\cdots\text{Te}$  interactions.<sup>42</sup> The  $\text{Te}\cdots\text{F}$  interactions described here are thus at the lower range of the already known noncovalent interactions involving a tellurium atom (Fig. 9).

## Conclusions

In conclusion, after having prepared new fluoro- and trifluoro tellurium derivatives, we demonstrated the presence of noncovalent  $\text{Te}\cdots\text{F}$  interactions through the  $\sigma$ -holes on tellurium and their importance in solution as indicated by  $^{19}\text{F}$  and  $^{125}\text{Te}$  NMR studies. The various effects reported here established the presence of ChB between Te and F as schematically shown in Fig. 3B.

By variable temperature experiments, we were even able to evaluate the intensity of such noncovalent  $\text{Te}\cdots\text{F}$  interactions ( $-3$  to  $-11$   $\text{kJ}\cdot\text{mol}^{-1}$ ). The identification of noncovalent  $\text{Te}\cdots\text{F}$  interactions reported here should provide new opportunities in organic chemistry, especially in organocatalysis, in drug design and in biology. Further work in these areas is underway in our group.

**Table 3** Thermodynamic parameters of the *anti-syn* equilibrium of tellurium derivatives **2**, **5a** and **5c**.<sup>a</sup>

Compound	$\Delta H \approx E_{\text{Te}\cdots\text{F}}$ ( $\text{kJ}\cdot\text{mol}^{-1}$ )	$\Delta S$ ( $\text{J}\cdot\text{K}^{-1}\cdot\text{mol}^{-1}$ )	$\Delta G^{298}$ ( $\text{kJ}\cdot\text{mol}^{-1}$ )
<b>2</b>	$-7.6 - -6.3$	$-21.3 - -15.5$	$-1.2 - -1.7$
<b>5a</b>	$-4.4 - -3.0$	$-20.7 - -17.0$	$+1.6 - +2.1$
<b>5c</b>	$-10.6 - -9.1$	$-29.5 - -22.4$	$-1.8 - -2.4$

<sup>a</sup> See ESI, Table S7 for full data.

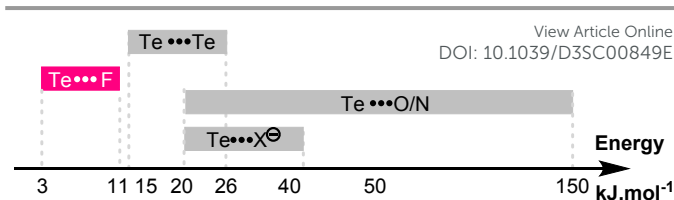


**Fig. 9** Energy range of the known noncovalent interactions involving tellurium atom and of the  $\text{Te}\cdots\text{F}$  interaction reported here.

## Data availability

Experimental and computational data associated with this work are provided in the accompanying ESI.

## Author Contributions

RW and LG carried out the experiments. EA performed the computational studies. RW, PP and VM designed the project. PP and VM co-wrote the manuscript. VM co-wrote and edited the ESI. RW and EA co-wrote the ESI and contributed to writing the manuscript.

## Conflicts of interest

There are no conflicts to declare

## Acknowledgements

This research was funded by the International Center Frontier Research in Chemistry (icFRC), the LabEx CSC (ANR-10-LABX-0026 CSC) and French National Research Agency (ANR-21-CE07-0014). RW thanks the LabEx CSC, Strasbourg, for a PhD fellowship and LG thanks the ANR for a PhD fellowship. We thank the EXPLOR mesocenter for providing access to their computing facility (project 2021CPMXX2483) and the NMR service (B. Vincent) of the LeBel Federation FR2010 for the easy access to the spectrometers and for advice. E.A. thanks Dr Axel Gansmüller for fruitful discussions.

## References

- (a) P. Politzer, J. S. Murray, T. Clark, *Phys. Chem. Chem. Phys.*, 2013, **15**, 11178–11588; (b) A. Bauzá, T. J. Mooibroek, A. Frontera, *ChemPhysChem*, 2015, **16**, 2496–2517.
- G. Cavallo, P. Metrangolo, R. Milani, T. Pilati, A. Priimagi, G. Resnati, G. Terraneo, *Chem. Rev.*, 2016, **116**, 2478–2601.
- For recent developments of XB applications in biology and in organic chemistry, see: (a) G. Berger, P. Frangville, F. Meyer, *Chem. Commun.*, 2020, **56**, 4970–4981; (b) R. L. Sutar, S. M. Huber, *ACS Catal.*, 2019, **9**, 9622–9639.
- ChB has been sparingly investigated in the last decade, see: (a) P. Scilabra, G. Terraneo, G. Resnati, *Acc. Chem. Res.*, 2019, **52**, 1313–1324; (b) N. Biot, D. Bonifazi, *Coord. Chem. Rev.*, 2020, **413**, 213243; (c) R. Hein, P. D. Beer, *Chem. Sci.*, 2022, **13**, 7098.
- A. Frontera, A. Bauzá, *Int. J. Mol. Sci.*, 2022, **23**, 4188.
- C. B. Aakeröy, D. L. Bryce, G. R. Desiraju, A. Frontera, A. C. Legon, F. Nicotra, K. Rissanen, S. Scheiner, G. Terraneo, P.



- Metrangolo, G. Resnati, *Pure Appl. Chem.*, 2019, **91**, 1889–1892.
- 7 (a) M. R. Scholfield, C. M. Vander Zanden, M. Carter, P. S. Ho, *Prot. Sci.*, 2013, **22**, 139–152; (b) P. S. Ho, *Future Med. Chem.*, 2017, **4**, 637–640.
- 8 (a) M. Iwaoka, N. Isozumi, *Molecules*, 2012, **17**, 7266–7283; (b) K. Kriz, J. Fanfrik, M. Lepsik, *ChemPhysChem*, 2018, **19**, 2540–2548.
- 9 E. R. T. Tiekink, *Dalton Trans.*, 2012, **41**, 6390–6395.
- 10 (a) P. Shah, A. D. Westwell, *J. Enz. Inhib. Med. Chem.*, 2007, **22**, 527–540; (b) I. Ojima, Ed., *Fluorine in Medicinal Chemistry and Chemical Biology*, Wiley-Blackwell, 2009.
- 11 W. Pietrus, R. Kafel, A. J. Bojarski, R. Kurczab, *Molecules*, 2022, **27**, 1005–1019.
- 12 The actual presence of XB with F atom is still a matter of debate; see ref. 2 and: (a) P. Metrangolo, J. S. Murray, T. Pilati, P. Politzer, G. Resnati, G. Terraneo, *Cryst. Growth Des.*, 2011, **11**, 4238–4246; (b) K. Eskandari, M. Lesani, *Chem. Eur. J.*, 2015, **21**, 4739–4746; (c) S. Scheiner, *J. Phys. Chem. A*, 2020, **124**, 7290–7299; (d) S. A. Harry, S. Vemulapalli, T. Dudding, T. Lectka, *J. Org. Chem.*, 2022, **13**, 8413–8419.
- 13 K. Grollier, A. Taponard, T. Billard, *Eur. J. Org. Chem.*, 2020, **2020**, 6943–6954.
- 14 For a study on the Se-F interaction, see: M. Iwaoka, H. Komatsu, T. Katsuda, S. Tomoda, *J. Am. Chem. Soc.*, 2002, **124**, 1902–1909.
- 15 Pauling electronegativity of halogens: F 4.0, Cl 3.0, Br 2.8, I 2.5, of chalcogens: O 3.5, S 2.5, Se 2.4, Te 2.1.
- 16 P. Politzer, P. Lane, M. C. Concha, Y. Ma, J. S. Murray, *J. Mol. Model.*, 2007, **13**, 305–311.
- 17 B. Zhou, F. P. Gabbai, *Chem. Sci.*, 2020, **11**, 7495–7500.
- 18 P. Pale, V. Mamane, *ChemPhysChem*, 2023, **24**, e202200481.
- 19 (a) R. Weiss, E. Aubert, L. Gros Lambert, P. Pale, V. Mamane, *Chem. Eur. J.*, 2022, **28**, e202200395; (b) R. Weiss, E. Aubert, P. Pale, V. Mamane, *Angew. Chem. Int. Ed.*, 2021, **60**, 19281–19286; (c) H. Nishiyama, F. Zheng, S. Inagi, H. Fueno, K. Tanaka, I. Tomita, *Polym. Chem.*, 2020, **11**, 4693–4698; (d) S. Mehrparvar, C. Wölper, R. Gleiter, G. Haberhauer, *Angew. Chem. Int. Ed.*, 2020, **59**, 17154–17161; (e) L. Chen, J. Xiang, Y. Zhao, Q. Yan, *J. Am. Chem. Soc.*, 2018, **140**, 7079–7082; (f) E. Pietrasiak, A. Togni, *Organometallics*, 2017, **36**, 3750–3757; (g) P. C. Ho, P. Szydlowski, J. Sinclair, P. J. W. Elder, J. Kübel, C. Gendy, L. M. Lee, H. Jenkins, J. F. Britten, D. R. Morim, I. Vargas-Baca, *Nat. Commun.*, 2016, **7**, 11299; (h) P. R. Prasad, K. Selvakumar, H. B. Singh, R. J. Butcher, *J. Org. Chem.*, 2016, **81**, 3214–3226; (i) M. Baiwir, G. Llabres, J. Denoel, J.-L. Piette, *Mol. Phys.*, 1973, **25**, 1–7.
- 20 (a) T. Glodde, Y. V. Vishnevskiy, L. Zimmermann, H.-G. Stamm, B. Neumann, N. W. Mitzel, *Angew. Chem. Int. Ed.*, 2021, **60**, 1519–1523; (b) M. Hejda, D. Duvinage, E. Lork, R. Jirásko, A. Lyčka, S. Mebs, L. Dostál, J. Beckmann, *Organometallics*, 2020, **39**, 1202–1212; (c) I. D. Sadekov, V. I. Minkin, A. V. Zakharov, A. G. Starikov, G. S. Borodkin, S. M. Aldoshin, V. V. Tkachev, G. V. Shilov, F. J. Berry, *J. Organomet. Chem.*, 2005, **690**, 103–116; (d) A. G. Maslakov, W. R. McWhinnie, M. C. Perry, N. Shaikh, S. L. W. McWhinnie, T. A. Hamor, *J. Chem. Soc. Dalton Trans.*, 1993, 619–624.
- 21 (a) M. Bühl, F. R. Knight, A. Křístková, I. M. Ondík, O. L. Malkina, R. A. M. Randall, A. M. Z. Slawin, J. D. Woollins, *Angew. Chem. Int. Ed.*, 2013, **52**, 2495–2498; (b) F. R. Knight, L. M. Diamond, K. S. Athukorala Arachchige, P. Sanz Camacho, R. A. M. Randall, S. E. Ashbrook, M. Bühl, A. M. Z. Slawin, J. D. Woollins, *Chem. Eur. J.*, 2015, **21**, 3613–3627; (c) M. W. Stanford, F. R. Knight, K. S. A. Arachchige, P. S. Camacho, S. E. Ashbrook, M. Bühl, A. M. Z. Slawin, J. D. Woollins, *Dalton Trans.*, 2014, **43**, 6548–6560.
- 22 (a) A. Nordheider, E. Hupf, B. A. Chalmers, F. R. Knight, M. Bühl, S. Mebs, L. Chęcińska, E. Lork, P. S. Camacho, S. E. Ashbrook, K. S. Athukorala Arachchige, D. B. Cordes, A. M. Z. Slawin, J. Beckmann, J. D. Woollins, *Inorg. Chem.*, 2015, **54**, 2435–2446; (b) T. G. Do, E. Hupf, A. Nordheider, E. Lork, A. M. Z. Slawin, S. G. Makarov, S. Yu. Ketkov, S. Mebs, J. D. Woollins, J. Beckmann, *Organometallics*, 2015, **4**, 5341–5360.
- 23 K. T. Mahmudov, A. V. Gurbanov, V. A. Aliyeva, M. F. C. Guedes da Silva, G. Resnati, A. J. L. Pombeiro, *Coord. Chem. Rev.*, 2022, **464**, 214556.
- 24 (a) H. Zhao, F. P. Gabbai, *Nature Chem.*, 2010, **2**, 984–990; (b) J. Y. C. Lim, I. Marques, A. L. Thompson, K. E. Christensen, V. Felix, P. D. Beer, *J. Am. Chem. Soc.*, 2017, **139**, 3122–3133.
- 25 A. Dessì, P. Peluso, R. Dallochio, R. Weiss, G. Andreotti, M. Allocca, E. Aubert, P. Pale, V. Mamane, S. Cossu, *Molecules*, 2020, **25**, 2213.
- 26 (a) P. Peluso, V. Mamane, A. Dessì, R. Dallochio, E. Aubert, C. Gatti, D. Mangelings, S. Cossu, *J. Chromatog. A*, 2020, **1616**, 460788; (b) P. Peluso, C. Gatti, A. Dessì, R. Dallochio, R. Weiss, E. Aubert, P. Pale, S. Cossu, V. Mamane, *J. Chromatog. A*, 2018, **1567**, 119–129; (c) R. Dallochio, A. Dessì, M. Solinas, A. Arras, S. Cossu, E. Aubert, V. Mamane, P. Peluso, *J. Chromatog. A*, 2018, **1563**, 71–81; (d) P. Peluso, V. Mamane, R. Dallochio, A. Dessì, R. Villano, D. Sanna, E. Aubert, P. Pale, S. Cossu, *J. Sep. Sci.*, 2018, **41**, 1247–1256; (e) P. Peluso, V. Mamane, E. Aubert, A. Dessì, R. Dallochio, A. Dore, P. Pale, S. Cossu, *J. Chromatog. A*, 2016, **1467**, 228–238.
- 27 (a) R. Weiss, E. Aubert, P. Peluso, S. Cossu, P. Pale, V. Mamane, *Molecules*, 2019, **24**, 4484; (b) V. Mamane, P. Peluso, E. Aubert, R. Weiss, E. Wenger, S. Cossu, P. Pale, *Organometallics*, 2020, **39**, 3936–3950; (c) R. Weiss, T. Golisano, P. Pale, V. Mamane, *Adv. Synth. Catal.*, 2021, **363**, 4779–4788; (d) E. Aubert, A. Doudouh, E. Wenger, B. Sechi, P. Peluso, P. Pale, V. Mamane, *Eur. J. Inorg. Chem.*, 2022, **2022**, e202100927; (e) L. Gros Lambert, A. Padilla-Hernandez, R. Weiss, P. Pale, V. Mamane, *Chem. Eur. J.*, 2023, **29**, e202203372.
- 28 (a) For a general review on the importance of through-space spin-spin coupling in NCI, see: J.-C. Hierso, *Chem. Rev.*, 2014, **114**, 4838–4867; (b) For a recent study using  $^{19}\text{F}$  NMR to probe the XB through determination of through-bond  $^1\text{J}_{\text{C-F}}$  couplings, see: B. Jimmink, D. Sethio, L. Turunen, D. von der Heiden, M. Erdélyi, *J. Am. Chem. Soc.*, 2021, **143**, 10695–10699.
- 29 (a) H. B. Singh, N. Sudha, A. A. West, T. A. Hamor, *J. Chem. Soc., Dalton Trans.*, 1990, 907–913; (b) For an overview, see: H. B. Singh, G. Mugesh, *Acc. Chem. Res.*, 2002, **35**, 226–236.
- 30 R. Weiss, Y. Cornaton, H. Khartabil, L. Gros Lambert, E. Hénon, P. Pale, J.-P. Djukic, V. Mamane, *ChemPlusChem*, 2022, **87**, e202100518.
- 31 S. Saba, J. Rafique, A. L. Braga, *Adv. Synth. Catal.*, 2015, **357**, 1446–1452.
- 32 A. Ouchi, T. Hyugano, C. Liu, *Org. Lett.* 2011, **11**, 4870–4873.
- 33 A. Panda, H. B. Singh, *NMR of Organoselenium and Organotellurium Compounds*, PATAI'S Chemistry of Functional Groups, John Wiley & Sons, Ltd, 2013.
- 34 A. Hammerl, T. M. Klapötke, B. Krumm, M. Scherr, *Z. Anorg. Allg. Chem.*, 2007, **633**, 1618–1626.
- 35 (a) F. B. Mallory, E. D. Luzik Jr. C. W. Mallory, P. J. Carroll, *J. Org. Chem.*, 1992, **57**, 366–370; (b) F. B. Mallory, C. W. Mallory, K. E. Butler, M. B. Lewis, A. Q. Xia, E. D. Luzik Jr., L. E. Fredenburgh, M. M. Ramanjulu, Q. N. Van, M. M. Francl, D. A. Freed, C. C. Wray, C. Hann, M. Nerz-Stormes, P. J. Carroll, L. E. Chirlian, *J. Am. Chem. Soc.*, 2000, **122**, 4108–4116.
- 36 S. Grzesiek, F. Cordier, V. Jaravine, M. Barfield, *Prog. Nucl. Magn. Reson.*, 2004, **45**, 275–300.
- 37 L. Ernst, K. Ibrom, *Angew. Chem. Int. Ed.*, 1995, **34**, 1881–1882.
- 38 For comparison, see the  $^n\text{J}_{\text{C-F}}$  coupling in trifluorotoluene (Hz):  $^1\text{J}_{\text{C-F}} = 272$ ;  $^2\text{J}_{\text{C-F}} = 32$ ;  $^3\text{J}_{\text{C-F}} = 4$ ;  $^4\text{J}_{\text{C-F}} = 1$ ;  $^5\text{J}_{\text{C-F}} = 0$ .



- 39 C. Otake, T. Namba, H. Tabata, K. Makino, K. Hirano, T. Oshitari, H. Natsugari, T. Kusumi, H. Takahashi, *J. Org. Chem.*, 2021, **86**, 4638–4645.
- 40 R. Ramalakshmi, K. Saha, D. K. Roy, B. Varghese, A. K. Phukan, S. Ghosh, *Chem. Eur. J.*, 2015, **21**, 17191–17195.
- 41 The chemical shift for **10-Li** ( $\delta_{\text{Te}} = 105.8$  ppm) is in the same range as for the known PhTeLi ( $\delta_{\text{Te}} = 133.9$  ppm), see: M. A. Banks, O. T. Beachley, H. J. Gysling and H. R. Luss, *Organometallics*, 1990, **9**, 1979–1982.
- 42 R. Gleiter, G. Haberhauer, D. B. Werz, F. Rominger, C. Bleiholder, *Chem. Rev.*, 2018, **118**, 2010–2041.

View Article Online  
DOI: 10.1039/D3SC00849E

